# Probing the spin-glass freezing transition in $Cu_{1-x}Mn_x$ alloy by spin current

Po-Hsun Wu,[1] Yen-Chang Tu,[1] Danru Qu,[2,*] Hsia-Ling Liang,[1] Shang-Fan Lee,[2] and Ssu-Yen Huang[1,†]
[1]*Department of Physics, National Taiwan University, Taipei 16017, Taiwan*
[2]*Institute of Physics, Academia Sinica, Taipei 11529, Taiwan*

(Received 14 September 2019; revised manuscript received 21 February 2020; accepted 25 February 2020; published 12 March 2020)

In this study, we used the thermally driven spin current to investigate the spin frustrations and spin fluctuations in spin-glass (SG) $Cu_{1-x}Mn_x$ alloys. Tuning the $Cu_{1-x}Mn_x$ composition results in a transition of the alloys from the SG state to the antiferromagnetic state; these states have different spin-freezing temperatures ($T_f$). Most spins randomly freeze at temperatures lower than the $T_f$ of the alloy. For each alloy composition, we obtained a temperature-dependent inverse spin Hall voltage with a peak at $T_p$. Crucially, $T_p$ had nearly identical composition dependence as that of $T_f$,, with $T_p$ being nine times larger than $T_f$. Similar behavior was captured using the SG insulator, amorphous $Y_3Fe_5O_{12}$. These results indicated that the maximum spin fluctuation in both conducting and insulating SGs occurred at temperatures considerably higher than the $T_f$ of each. In addition, we demonstrated the importance of the effective number of valence electrons in tailoring the spin Hall angle in binary alloys.

DOI: 10.1103/PhysRevB.101.104413

## I. INTRODUCTION

The exploitation of pure spin current with a flow of spin angular momentum is a promising alternative to traditional charged-based electronic devices to keep pace with Moore's law. Numerous studies have focused on the efficient generation and manipulation of spin current for spintronic devices. An effective approach to enhance the spin current is through spin fluctuations (SFs) [1,2]. During magnetic phase transition, magnetic systems evolve from the long-range ordered magnetic state into the disordered state and exhibit short-range SFs. Several researchers have demonstrated an increase in the spin current near the phase transition temperature in magnetic systems such as the weak ferromagnetic (FM) metal NiPd [3]; the antiferromagnetic (AFM) insulators NiO [4,5], CoO [6], and $Cr_2O_3$ [7]; the AFM metal IrMn [8,9]; and the FM alloy $Fe_xPt_{1-x}$ [10]. Spin-current enhancement in these long-range ordered magnetic systems during SF suggests that the short-range ordered spin-glass (SG) system can possibly be enhanced because the frustrated intrachain coupling in SG has a significant short-range order that induces large fluctuations [11].

In SG materials, magnetic ions are randomly distributed among the host nonmagnets. When cooled from the paramagnetic state, the SG materials exhibit a nontrivial spin-freezing transition, where spins start to align in random directions and slowly reach a glassy state. Injecting spin current into SG materials has been previously studied using FM-resonance-driven spin pumping [12] and nonlocal spin valve [13] measurements. However, the results were contradictory with the strong enhancement observed in spin pumping and the strong suppression observed in nonlocal spin valve measurements.

To understand the interplay between spin current and SG systems, we studied the temperature dependence of the injection of spin current from the FM insulator $Y_3Fe_5O_{12}$ (YIG) into SG $Cu_{1-x}Mn_x$ alloys with various compositions and under a range of temperatures including their phase transitions. $Cu_{1-x}Mn_x$ alloys possess rich magnetic phases, as depicted in Fig. 1(a). When the concentration of Mn increases, its magnetic phase changes from SG to AFM. By measuring zero-field-cooled (ZFC) and field-cooled (FC) magnetization, we obtained the spin-freezing temperature ($T_f$), the temperature at which the ZFC and FC curves bifurcate and exhibit irreversible behavior. By utilizing the spin Seebeck effect (SSE) in YIG, we measured the temperature-dependent ($T$-dependent) inverse spin Hall-effect (ISHE) voltage of $Cu_{1-x}Mn_x$ alloys. Crucially, for each composition, a voltage peak ($T_p$) was observed, and it exhibited almost identical composition dependence as that of $T_f$, thus revealing a strong correlation between $T_p$ and $T_f$. A similar behavior was also captured using the SG insulator, amorphous YIG ($a$-YIG). Further, we demonstrated that all results followed a universal curve in a scaling plot based on spin susceptibility, which agreed with the three-dimensional (3D) Ising model and supported the finding of a strong short-range correlation during spin fluctuation. Thus, examining spin-current injection and spin-to-charge conversion is a simple, viable, and convenient means of electrically investigating the complex spin-freezing process in magnetically short-range ordered SG materials. Similarly, the SSE was also recently used to investigate the short-range magnetic order in frustrated magnetic $Gd_3Ga_5O_{12}$, discovered recently by [14].

## II. EXPERIMENT

We used magnetron cosputtering to deposit thin films of $Cu_{1-x}Mn_x$ alloys onto polycrystalline YIG substrates. To prevent oxidation, a 2-nm-thick $Al_2O_3$ layer was deposited

*danru@gate.sinica.edu.tw
†syhuang@phys.ntu.edu.tw

 

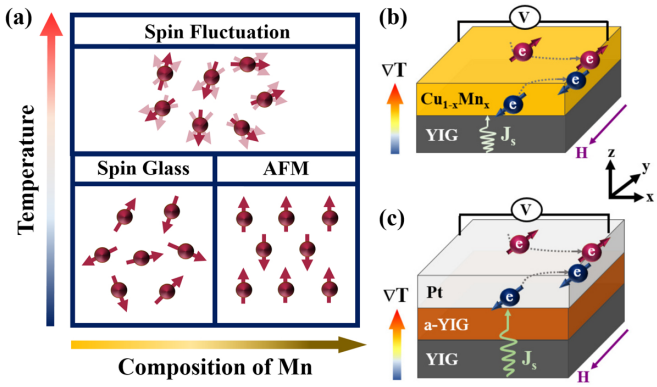


FIG. 1. (a) Schematic of the magnetic ordering from spin glass to the antiferromagnetic state by increasing composition of Mn and from the magnetically ordered state to the spin-fluctuation state by increasing temperature. Schematic of the spin-current transmission through (b) SG metal and (c) SG insulator using the ISHE/SSE measurement.

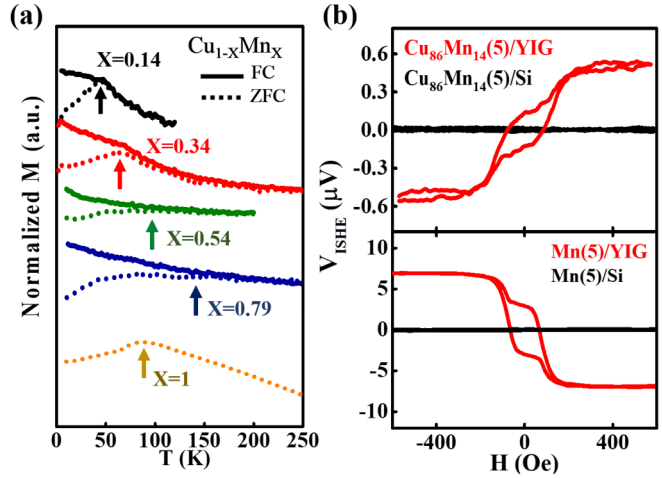


FIG. 2. (a) ZFC (dashed curve) and FC (solid curve) temperature-dependent magnetization for $Cu_{1-x}Mn_x(300)/Si$ with $x = 0.14$ (black), 0.34 (red), 0.54 (green), 0.79 (blue), and 1 (yellow). Arrows indicate the corresponding spin-freezing temperature ($T_f$) for each composition. (b) Field-dependent ISHE voltage for $Cu_{86}Mn_{14}(5)$/YIG (upper red), $Cu_{86}Mn_{14}(5)$/Si (upper black), Mn(5)/YIG (lower red), and Mn(5)/Si (lower black) at room temperature.

to be the top layer. The composition of the $Cu_{1-x}Mn_x$ films was precisely determined using the electron probe x-ray microanalyzer. For magnetization measurement, we fabricated 300-nm-thick $Cu_{1-x}Mn_x$ on oxidized Si substrates. For ISHE/SSE measurement, 5- to 100-nm-thick $Cu_{1-x}Mn_x$ films were prepared. In addition, 1- to 300-nm-thick *a*-YIG thin films were deposited at room temperature on the oxidized Si and YIG slab through rf sputtering.

## III. RESULTS AND DISCUSSION

The *T*-dependent ZFC and FC magnetization of $Cu_{1-x}Mn_x$ were measured using a superconducting quantum interference device. In the ZFC process, the sample was cooled to 5 K without using an external magnetic field. Then, magnetization was measured by raising the temperature to 300 K under 100 Oe. In the FC process, the sample was cooled from 300 to 5 K under the magnetic field, and the magnetization was measured with the same field. A pronounced cusp, corresponding to $T_f$ and featuring the canonical SG behavior [15], was observed for 14 and 34% Mn at 45 and 67 K, respectively, as depicted in Fig. 2(a). For 54.3 and 79.4% Mn, the ZFC peak was broader and the bifurcation occurred at a higher temperature. This was possibly because of the mixing of the short-range and long-range orderings [15]. Because irreversibility is a distinctive feature of SG materials, we recorded temperatures at bifurcation as $T_f$, and these temperatures were 100 and 160 K for 54.3 and 79.4% Mn, respectively. For pure Mn, the ZFC peak at 90 K was consistent with its Néel temperature ($T_N$; for simplicity, we use $T_f$ hereafter) [16]. Therefore, an increase in Mn content resulted in an increase in $T_f$, reaching a maximum at $x = 79.4\%$, and then a decrease.

We next measured the ISHE/SSE voltage for these samples. In ISHE/SSE measurement, the sample was placed between the resistance heater and the Cu block (heat sink) to generate a temperature gradient along the *z* axis, and the voltage was measured along the *y* axis under an external field along the *x* axis, as depicted in Fig. 1(a) [17,18]. We first present the spin-dependent thermal voltages for SG $Cu_{86}Mn_{14}(5)$/YIG and AFM Mn(5)/YIG (numbers in parentheses are thicknesses in nanometers) in Fig. 2(b). Compared with $Cu_{86}Mn_{14}$/YIG with $|V_{ISHE}| = 0.5\,\mu V$, a larger value of approximately $7\,\mu V$ was observed in Mn/YIG. In the low-field region, a plateau behavior was observed because of noncollinear YIG surface magnetization [19]. The controlled samples, $Cu_{86}Mn_{14}(5)$/Si and Mn(5)/Si, exhibited no measurable thermal voltages; thus, the contribution of anomalous Nernst effect was not present in these films. Notably, the $V_{ISHE}$ of $Cu_{86}Mn_{14}$/YIG had an opposite sign to that of Mn/YIG. The sign of $\vartheta_{SH}$ for binary alloys depends on the effective number of their valence electrons. This is discussed later.

Spin-current enhancement during spin-freezing transition is captured by the *T*-dependent $V_{ISHE}$ of SG $Cu_{86}Mn_{14}$/YIG with various thicknesses. As depicted in Fig. 3(a), $|V_{ISHE}|$ first increased, reaching a maximum of approximately $T_p = 90$ K and revealing the influence of SF, and then decreased along with temperature. Notably, $T_p$ was not equal to $T_f$ but was approximately two times larger, as depicted in Fig. 3(c). $T_f$ and $T_p$ were observed on 300- and 5-nm-thick films, respectively. According to finite-size scaling theory, the 5-nm film could have lower $T_f$ than 300-nm film, as indicated in the following expression [20,21]:

$$\frac{T_f(\infty) - T_f(t)}{T_f(\infty)} = \left(\frac{\xi_0}{t}\right)^{\lambda} \quad (1)$$

Here, $T_f(\infty)$ is the bulk spin-freezing (or Néel for antiferromagnet) temperature, $t$ is the thickness, $\lambda = 0.75$ is the shift exponent, and $\xi_0 = 3.52$ nm is the spin-correlation length, obtained from Refs. [21,22]. Therefore, after considering the finite-size effect, we obtained a $T_f$ (5 nm) of approximately 11 K, which was approximately nine times smaller than the $T_p$ for the same thickness. The considerable

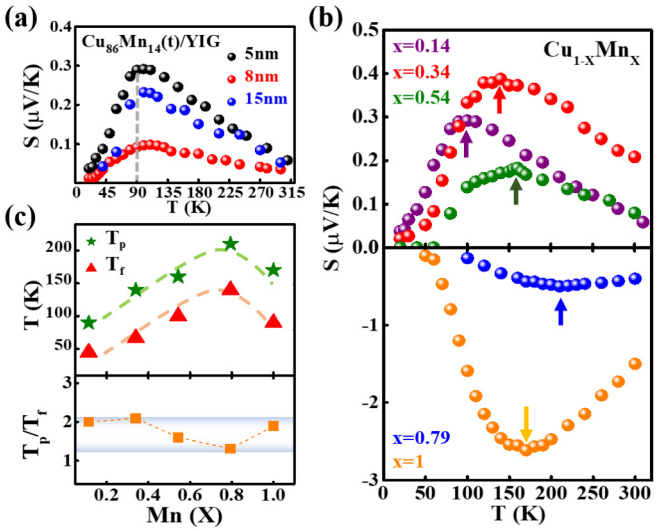


FIG. 3. (a) Temperature-dependent spin Seebeck coefficient for 5-nm- (black), 8-nm- (red), and 15-nm-thick (blue) $Cu_{86}Mn_{14}$. (b) Temperature-dependent spin Seebeck coefficient for $Cu_{1-x}Mn_x$ with $x = 0.14$ (black), 0.34 (red), 0.54 (green), 0.79 (blue), and 1 (yellow). Arrows indicate the voltage peak at $T_p$. (c) Plots of $T_p$ (green star), $T_f$ (red triangle), and $T_p/T_f$ (yellow square) on $Cu_{1-x}Mn_x$ compositions.

difference in $T_p$ and $T_f$ was not entirely unexpected. Studies on SG that used the neutron spin echo, Mossbauer effect, and muon spin-relaxation techniques have reported that the onset of the complex spin-freezing process is considerably higher than $T_f$ [9,23,24]. The approximate ratio of $T_p/T_f$ (5 nm) obtained in our study was 9, which is consistent with these reports and indicates that the maximum SF in SG occurs at a temperature considerably higher than $T_f$. Compared with the aforementioned sophisticated techniques, the proposed method is a considerably simple and convenient electrical method for investigating the complex spin-freezing transition in SG.

Similar enhancement was also obtained for other compositions, as depicted in Fig. 3(b). For $Cu_{1-x}Mn_x$ alloys with $x = 14$, 34, 54, 79, and 100, $T_p$ was 90, 140, 160, 210, and 170 K, respectively, demonstrating an increasing trend followed by a decrease. The $T$-dependent ISHE/SSE behavior in Pt/YIG was attributed to the competition between magnon propagation length and the concentration of magnon in YIG [25]. However, the composition-dependent $T_p$ observed in our study clearly indicated that the magnonic spin current was strongly modulated by the SF in $Cu_{1-x}Mn_x$ alloys. Furthermore, although $T_f$ and $T_p$ presented almost identical composition dependence, $T_p$ was always larger (1.3–2.1 times) than $T_f$ in the compositions, as depicted in Fig. 3(c). Considering the finite-size effect, this ratio could be even larger. In addition, the $T_p$ for $Cu_{86}Mn_{14}$ was almost thickness independent, as illustrated in Fig. 3(a). This was because the film thickness was larger than the spin-correlation length $\xi_0$.

We used critical theory to understand the continuous phase transition in $Cu_{1-x}Mn_x$ [26]. In critical theory, the magnetic susceptibility $\chi$ follows the relation $\frac{\chi}{ft^{\gamma}} = \frac{h}{t^{\gamma+\beta}}$, where $h = \frac{H}{k_B T}$, $\beta$ and $\gamma$ are the critical exponents for spontaneous

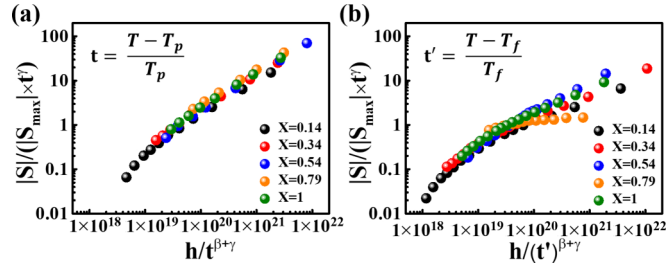


FIG. 4. Scaling plot of the normalized spin Seebeck coefficient by the 3D Ising critical exponent with (a) $T_{\text{critical}} = T_p$ and (b) $T_{\text{critical}} = T_f$ for $Cu_{1-x}Mn_x$ over the entire range of compositions.

staggered magnetization, $t = \frac{T - T_{\text{critical}}}{T_{\text{critical}}}$ is the reduced temperature for $T > T_{\text{critical}}$, and $f$ is the scaling function. A previous study [27] showed that the spin Seebeck coefficient ($S$) scales with magnetic susceptibility at temperatures higher than the AFM transition temperature. For SG, similarly, we plotted $\frac{|S|}{|S_{\max}|t^{\gamma}}$ versus $\frac{h}{t^{\gamma+\beta}}$, as depicted in Fig. 4, where $S$ is normalized by dividing its peak value $|S_{\max}|$. For $T_{\text{critical}} = T_p$, data collapse onto a single curve, but for $T_{\text{critical}} = T_f$,, data diverge at temperatures close to $T_{\text{critical}}$, as depicted in Figs. 4(a) and 4(b), respectively. Therefore, our analysis demonstrated that $S$ scales with spin susceptibility better than with the magnetic susceptibility and $T_p$ obtained from the SSE measurement represents the critical point of spin susceptibility during the continuous phase transition.

In addition, we calculated $\vartheta_{\text{SH}}$ and spin-diffusion length ($\lambda_{\text{SD}}$) for canonical SG $Cu_{86}Mn_{14}$ and AFM Mn by fitting the thickness ($t$)-dependent electrical resistivity ($\rho$) and $V_{\text{ISHE}}$ using Eq. (2) [28,29]:

$$\Delta V_{\text{ISHE}}(t) = 2CL\nabla T\,\rho(t)\theta_{\text{SH}}\frac{\lambda_{\text{sd}}}{t}\tanh\left(\frac{t}{2\lambda_{\text{sd}}}\right) \qquad (2)$$

Here, $L = 4$ mm is the distance between the voltage terminals, $\nabla T = 12\,\text{K/mm}$ is the temperature gradient, and $C$ is the spin-current injection coefficient. We use $C(\text{Mn}) = 3.5\,\text{Am}^{-1}\,\text{K}^{-1}$ for Mn [30] and $C(\text{Cu}_{86}\text{Mn}_{14}) = 1.5\,\text{Am}^{-1}\,\text{K}^{-1}$ for $Cu_{86}Mn_{14}$ [31]. From the fitting in Figs. 5(a) and 5(b), we obtained $\theta_{\text{SH}}(Cu_{86}Mn_{14}) = 6.94 \pm 1.33\%$, $\theta_{\text{SH}}(\text{Mn}) = -3.70 \pm 1.5\%$, $\lambda_{\text{SD}}(Cu_{86}Mn_{14}) = 6.36 \pm 1.85$ nm, and $\lambda_{\text{SD}}(\text{Mn}) = 2.89 \pm 1.35$ nm. Because Cu has negligible $\theta_{\text{SH}}$, the large $\theta_{\text{SH}}$ in 14% Mn-doped Cu with an *opposite* sign to pure Mn was notable. We further measured $\Delta V_{\text{ISHE}}$ for 5-nm-thick $Cu_{1-x}Mn_x$ over the entire composition. As depicted in Fig. 5(d), $\rho$ increased linearly with $x$. We plot $\Delta V_{\text{ISHE}}/\rho$ versus composition in Fig. 5(c) because it is proportional to $\theta_{\text{SH}}$. When adding Mn into Cu, $\Delta V_{\text{ISHE}}/\rho$ gradually increased and reached the positive maximum at $x = 34\%$, then decreased and crossed zero at approximately $x = 60\%$; it finally reached the negative maximum at $x = 100\%$, as depicted in Fig. 5(c). For a single $3d$ transition metal, when the total number of valence $3d$ and $4s$ electrons ($n_{3d+4s}$) is smaller (larger) than 8–9, the sign of $\theta_{\text{SH}}$ is positive (negative) [31]. This criterion also works for binary alloys. The effective $n_{3d+4s}$ for $Cu_{1-x}Mn_x$ alloy is as follows:

$$n_{3d+4s}(Cu_{1-x}Mn_x) = 11 \times (1-x) + 7 \times x = 11 - 4x. \qquad (3)$$

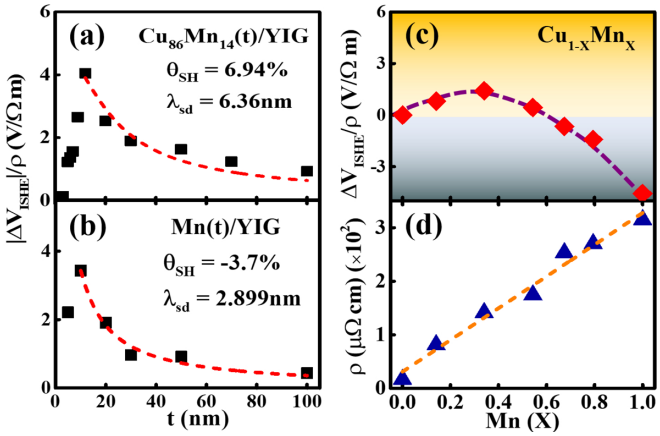


FIG. 5. Thickness-dependent $|\Delta V_{\mathrm{ISHE}}|/\rho$ for (a) $Cu_{86}Mn_{14}$ $(t)$/YIG and (b) Mn$(t)$/YIG. Red dashed line is the fitting curve determined by Eq. (2). Plot of (c) $|\Delta V_{\mathrm{ISHE}}|/\rho$ and (d) resistivity as a function of $Cu_{1-x}Mn_x$ composition.

According to the empirical criterion, $\theta_{\mathrm{SH}}$ changes sign at $n_{3d+4s} = 8-9$, corresponding to $x = 0.5-0.75$, and is consistent with our result ($x$ is approximately 0.6). We thus confirmed that the effective total number of *3d* and *4s* valence electrons is crucial in tuning and determining the sign of $\theta_{\mathrm{SH}}$ for binary alloys.

In addition to the conducting SG, we studied the spin-current enhancement in the insulating SG *a*-YIG, which possesses strong local negative exchange interaction but exhibits no long-range order, resulting in SG-like behavior. We fabricated *a*-YIG(300)/Si and determined its $T_f$ to be 50 K from the ZFC and FC curves under 1 T, as depicted in Fig. 6(a). The insertion of *a*-YIG between Pt and YIG enables the spin-current transmission through an SG insulator to be detected by measuring the ISHE/SSE. Notably, although a conventional insulating layer, such as $SiO_2$ or MgO at thickness of only a few nanometers, readily blocked the spin current, $V_{\mathrm{ISHE}}$ was still detectable in Pt/*a*-YIG $(t)$/YIG even when the *a*-YIG layer was as thick as 10 nm at 300 K, as depicted in Fig. 6(b). We extracted the $\lambda_{\mathrm{SD}}$ using the following simple estimation equation:

$$V_{\mathrm{ISHE}}(t)/V_{\mathrm{ISHE}}(0) = Ae^{-t/\lambda_{\mathrm{SD}}} \tag{4}$$

where $A$ is a constant and $t$ is the thickness of the *a*-YIG layer. The $\lambda_{\mathrm{SD}}$(*a*-YIG) was approximately 4.5 nm and considerably longer than $\lambda_{\mathrm{SD}}(SiO_2) = 0.06$ nm, as depicted in Fig. 6(c), but considerably shorter than the recently reported micrometer-long spin transmission distance in *a*-YIG determined from nonlocal measurement [32]. We measured the $T$-dependent $V_{\mathrm{ISHE}}$ for Pt/YIG and Pt/*a*-YIG$(t)$/YIG, as depicted in Fig. 6(d). The $T_p$ of Pt(3)/YIG was 100 K and that of Pt(3)/*a*-YIG(5)/YIG is much higher at around 150 K. For 10-nm *a*-YIG, the signal was considerably suppressed with a markedly broader peak. Nevertheless, $T_p$ was still higher than $T_f$ for Pt/*a*-YIG/YIG, which was consistent with that for $Cu_{1-x}Mn_x$/YIG and indicated that the maximum SF in the insulating SG occurs at a temperature considerably higher than its magnetic transition temperature. Thus, we demonstrated the use of SSE evaluates the change of spin susceptibility during spin-freezing transition in both conducting and insulating SGs.

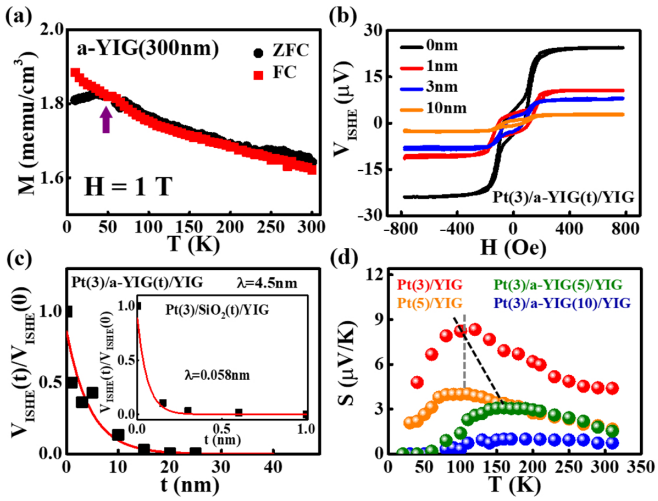


FIG. 6. (a) Temperature-dependent magnetization under ZFC (black) and FC (red) for *a*-YIG(300)/Si. (b) Field-dependent $V_{\mathrm{ISHE}}$ for Pt/*a*-YIG$(t)$/YIG. (c) Normalized $V_{\mathrm{ISHE}}$ for Pt/*a*-YIG$(t)$/YIG as a function of *a*-YIG thicknesses. Inset depicts normalized $V_{\mathrm{ISHE}}$ for Pt/$SiO_2(t)$/YIG as a function of $SiO_2$ thicknesses. Red curves are fittings from Eq. (4). (d) Temperature-dependent spin Seebeck coefficient for Pt(3)/YIG (red), Pt(5)/YIG (yellow), and Pt(3)/*a*-YIG$(t)$/YIG with $t = 0$ (red), 5 (green), and 10 nm (blue).

## IV. CONCLUSION

We studied the complex spin-freezing process through injecting spin current into the conducting SG $Cu_{1-x}Mn_x$ alloy. For each composition, we obtained $T_f$ and observed the pronounced enhancement in the $T$-dependent ISHE voltage with a peak at $T_p$. We demonstrated that $T_p$ has a strong correlation with $T_f$ because of almost identical composition dependence. Crucially, we provided direct evidence that the strongest spin fluctuation occurs at a temperature considerably higher than the magnetic critical temperature, which could be attributed to the long and complex spin-freezing process. Furthermore, we demonstrated that SSE measures the spin susceptibility during the spin-freezing process. A similar behavior was observed in the SG-like *a*-YIG insulator, thus demonstrating the versatility of this method. In addition, by estimating $\theta_{\mathrm{SH}}$ in $Cu_{1-x}Mn_x$, we confirmed the importance of the effective number of valence electrons in ISHE. The proposed approach utilizing the spin current is not only a promising alternative in studying the spin-freezing transition for SG but also may enable energy-efficient spintronic applications using SG materials.

## ACKNOWLEDGMENTS

The authors thank Cindy Huang, David Chien, and Wallace Academic Editing for English editing. This study was supported by the Ministry of Science and Technology of Taiwan under Grant No. MOST 106-2628-M-002-015-MY3. This study was also partially supported by Academia Sinica and National Taiwan University.

P.-H.W. and Y.-C.T. contributed equally to this work.

[1] V. Baltz, A. Manchon, M. Tsoi, T. Moriyama, T. Ono, and Y. Tserkovnyak, Rev. Mod. Phys. **90**, 015005 (2018).

[2] D. Hou, Z. Qiu, and E. Saitoh, NPG Asia Mater. **11**, 35 (2019).

[3] D. H. Wei, Y. Niimi, B. Gu, T. Ziman, S. Maekawa, and Y. Otani, Nat. Commun. **3**, 1058 (2012).

[4] H. Wang, C. Du, P. C. Hammel, and F. Yang, Phys. Rev. Lett. **113**, 097202 (2014).

[5] W. Lin, K. Chen, S. Zhang, and C. L. Chien, Phys. Rev. Lett. **116**, 186601 (2016).

[6] Z. Qiu, J. Li, D. Hou, E. Arenholz, A. T. N' Diaye, A. Tan, K.-i. Uchida, K. Sato, S. Okamoto, Y. Tserkovnyak, Z. Q. Qiu, and E. Saitoh, Nat. Commun. **7**, 12670 (2016).

[7] Z. Qiu, D. Hou, J. Barker, K. Yamamoto, O. Gomonay, and E. Saitoh, Nat. Mater. **17**, 577 (2018).

[8] L. Frangou, S. Oyarzún, S. Auffret, L. Vila, S. Gambarelli, and V. Baltz, Phys. Rev. Lett. **116**, 077203 (2016).

[9] J. Cramer, U. Ritzmann, B.-W. Dong, S. Jaiswal1, Z. Qiu, E. Saitoh, U. Nowak, and M. Kläui, J. Phys. D. Appl. Phys. **51**, 144004 (2018).

[10] Y. Ou, D. C. Ralph, and R. A. Buhrman, Phys. Rev. Lett. **120**, 097203 (2018).

[11] K. Binder and A. P. Young, Rev. Mod. Phys. **58**, 801 (1986).

[12] R. Iguchi, K. Ando, E. Saitoh, and T. Sato, J. Phys.: Conf. Ser. **266**, 012089 (2011).

[13] Y. Niimi, M. Kimata, Y. Omori, B. Gu, T. Ziman, S. Maekawa, A. Fert, and Y. Otani, Phys. Rev. Lett. **115**, 196602 (2015).

[14] C. Liu, S. M. Wu, J. E. Pearson, J. S. Jiang, N. d'Ambrumenil, and A. Bhattacharya, Phys. Rev. B **98**, 060415(R) (2018).

[15] P. Gibbs, T. M. Harders, and J. H. Smith, J. Phys. F: Met. Phys. **15**, 213 (1985).

[16] F. Boakye and G. Adanu, Thin Solid Films **279**, 29 (1996).

[17] Y.-J. Chen and S.-Y. Huang, Phys. Rev. Lett. **117**, 247201 (2016).

[18] F.-J. Chang, J. G. Lin, and S.-Y. Huang, Phys. Rev. Mater. **1**, 031401(R) (2017).

[19] P.-H. Wu and S.-Y. Huang, Phys. Rev. B **94**, 024405 (2016).

[20] T. Ambrose and C. Chien, Phys. Rev. Lett. **76**, 1743 (1996).

[21] G. G. Kenning, J. Bass, W. P. Pratt, Jr., D. Leslie-Pelecky, L. Hoines, W. Leach, M. L. Wilson, R. Stubi, and J. A. Cowen, Phys. Rev. B **42**, 2393 (1990).

[22] G. G. Kenning, J. M. Slaughter, and J. A. Cowen, Phys. Rev. Lett. **59**, 2596 (1987).

[23] K. Emmerich, E. Lippelt, R. Neuhaus, H. Pinkvos, C. Schwink, F. N. Gygax, A. Hintermann, A. Schenck, W. Studer, and A. J. van der Wal, Phys. Rev. B **31**, 7226 (1985).

[24] Y. J. Uemura, T. Yamazaki, D. R. Harshman, M. Senba, and E. J. Ansaldo, Phys. Rev. B **31**, 546 (1985).

[25] E.-J. Guo, J. Cramer, A. Kehlberger, C. A. Ferguson, D. A. MacLaren, G. Jakob, and M. Kläui, Phys. Rev. X **6**, 031012 (2016).

[26] N. Goldenfeld, *Lectures on Phase Transitions and the Renormalization Group*, 1st ed. (CRC Press, Boca Raton, FL, 2018).

[27] J. Li, Z. Shi, V. H. Ortiz, M. Aldosary, C. Chen, V. Aji, P. Wei, and J. Shi, Phys. Rev. Lett. **122**, 217204 (2019).

[28] D. Qu, S. Y. Huang, B. F. Miao, S. X. Huang, and C. L. Chien, Phys. Rev. B **89**, 140407(R) (2014).

[29] S. M. Rezende, R. L. Rodríguez-Suárez, R. O. Cunha, A. R. Rodrigues, F. L. A. Machado, G. A. Fonseca Guerra, J. C. Lopez Ortiz, and A. Azevedo, Phys. Rev. B **89**, 014416 (2014).

[30] D. Qu, T. Higo, T. Nishikawa, K. Matsumoto, K. Kondou, D. N.-Hamane, R. Ishii, P. K. Muduli, Y. Otani, and S. Nakatsuji, Phys. Rev. Mater. **2**, 102001(R) (2018).

[31] C. Du, H. Wang, F. Yang, and P. C. Hammel, Phys. Rev. B **90**, 140407(R) (2014).

[32] D. Wesenberg, T. Liu, D. Balzar, M. Wu, and B. L. Zink, Nat. Phys. **13**, 987 (2017).